Immunity, Volume *44*

Supplemental Information

NEMO Prevents RIP Kinase 1-Mediated Epithelial Cell Death and Chronic Intestinal Inflammation by NF-κB-Dependent and -Independent Functions

Katerina Vlantis, Andy Wullaert, Apostolos Polykratis, Vangelis Kondylis, Marius Dannappel, Robin Schwarzer, Patrick Welz, Teresa Corona, Henning Walczak, Falk Weih, Ulf Klein, Michelle Kelliher, and Manolis Pasparakis

Supplemental Data Figure 1

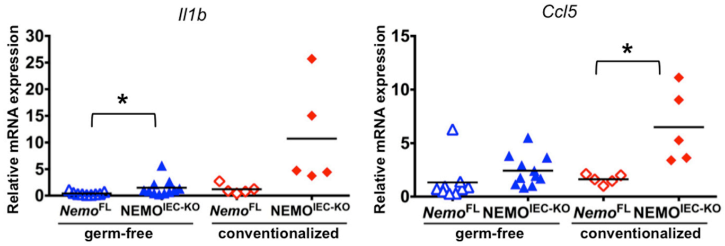

Figure S1 related to Figure 1

Inflammatory cytokine expression in NEMO^{IEC-KO} colons is driven by the microbiota

Graphs depicting relative mRNA expression levels of the indicated genes in colons of germ-free and conventionalized NEMO^{IEC-KO} and *Nemo*^{FL} mice (n = 5-11 mice per genotype).

Supplemental Data Figure 2

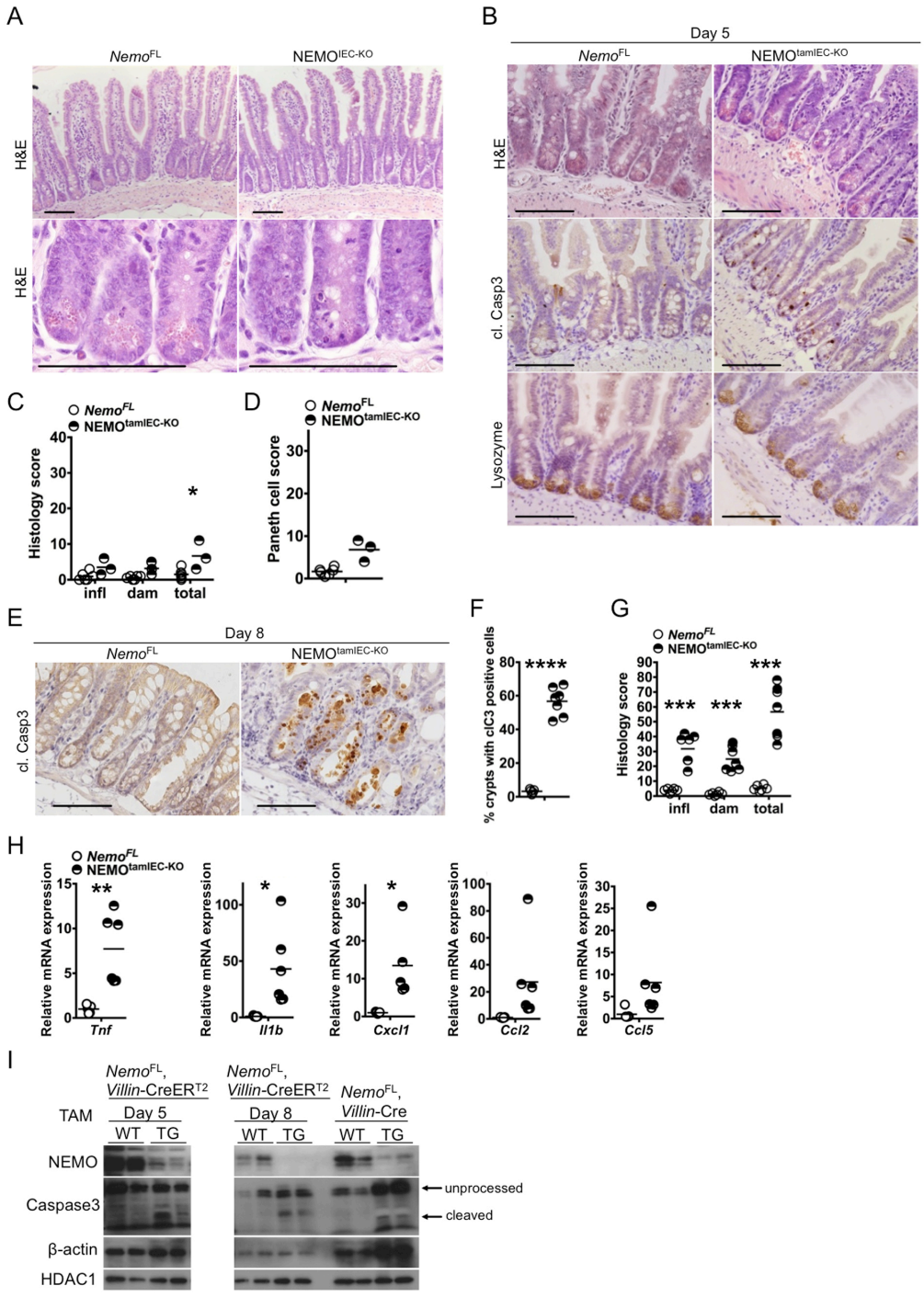

Figure S2 related to Figure 2

Paneth cell deficiency in NEMO^{IEC-KO} mice is a consequence of cell death

(A) Representative microscopy pictures of ileal sections from NEMO^{IEC-KO} and *Nemo*^{FL} mice stained with H&E at low and high power magnification.

(B) Representative images of ileal sections from NEMO$^{tamIEC-KO}$ and *Nemo*^{FL} mice 5 days after tamoxifen administration.

(C) Graph depicting histopathological scores of ileal sections from NEMO$^{tamIEC-KO}$ and *Nemo*^{FL} mice 5 days after tamoxifen administration (n = 3-6 mice per genotype).

(D) Graph depicting Paneth cell scores of ileal sections from NEMO$^{tamIEC-KO}$ and *Nemo*^{FL} mice 5 days after tamoxifen administration (n = 3-6 mice per genotype).

(E) Representative images of colon sections from NEMO$^{tamIEC\text{-}KO}$ and *Nemo*^{FL} mice on day 8 of tamoxifen administration immunostained for cl. casp3.

(F) Graph depicting percentage of crypts with cl. casp. 3 stained cells on colon sections of NEMO$^{tamIEC\text{-}KO}$ and *Nemo*^{FL} mice 8 days after tamoxifen administration (n = 5-6 mice per genotype).

(G) Graph depicting histopathological scores of colon sections from NEMO$^{tamIEC\text{-}KO}$ and *Nemo*^{FL} mice 8 days after tamoxifen administration (n = 6-7 mice per genotype).

(H) Graphs depicting mRNA levels of the indicated genes in the colon of NEMO$^{tamIEC\text{-}KO}$ and *Nemo*^{FL} littermates 8 days after tamoxifen administration (n = 5-6 mice per genotype).

(I) Immunoblot analysis of protein extracts from primary colon IECs from NEMO$^{tamIEC\text{-}KO}$ and *Nemo*^{FL} littermates 5 and 8 days after tamoxifen administration, and from *Nemo*^{FL} and NEMO $^{IEC\text{-}KO}$ mice probed with the indicated antibodies.

All scale bars represent 100μm.

Supplemental Data Figure 3

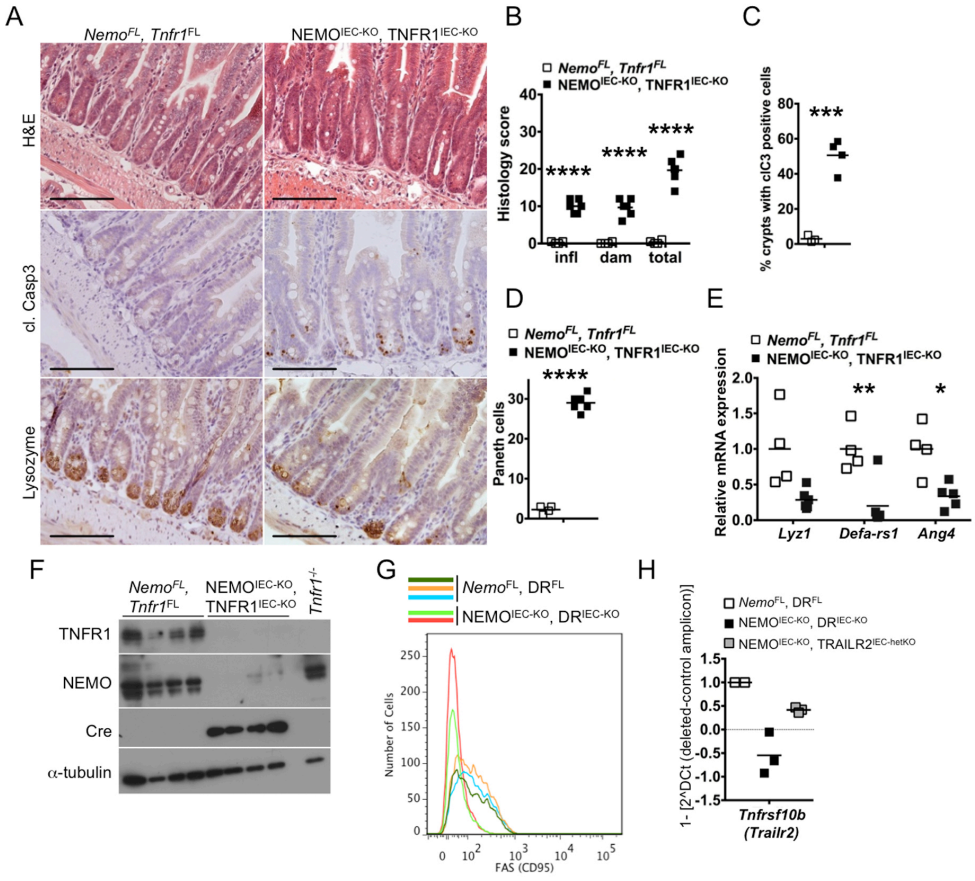

Figure S3 related to Figure 3

Deficiency of Paneth cells in NEMO^{IEC-KO} mice is not mediated by TNFR1 induced cell death

(A) Representative images of ileal sections from NEMO^{IEC-KO}, TNFR1^{IEC-KO} and *Nemo*^{FL}, *Tnfr1*^{FL} mice stained with H&E or immunostained for cl. casp3 or lysozyme.

(B) Graph depicting histopathological scores of ileal sections from NEMO^{IEC-KO}, TNFR1^{IEC-KO} and *Nemo*^{FL}, *Tnfr1*^{FL} mice (n = 4-6 mice per genotype).

(C) Graph depicting percentage of crypts with cl. casp 3 stained cells on ileal sections from NEMO^{IEC-KO}, TNFR1^{IEC-KO} and *Nemo*^{FL}, *Tnfr1*^{FL} mice (n = 3-4 mice per genotype).

(D) Graph depicting Paneth cell scores of ileal sections from NEMO^{IEC-KO}, TNFR1^{IEC-KO} and *Nemo*^{FL}, *Tnfr1*^{FL} mice (n = 4-6 mice per genotype).

(E) Graph depicting mRNA levels of the indicated genes in the ileum of NEMO^{IEC-KO}, TNFR1^{IEC-KO} and *Nemo*^{FL}, *Tnfr1*^{FL} mice (n = 4-6 mice per genotype).

(F) Immunoblot analysis of protein extracts from primary small intestinal IECs from NEMO^{IEC-KO}, TNFR1^{IEC-KO} and *Nemo*^{FL}, *Tnfr1*^{FL} mice with the indicated antibodies.

(G) Plot showing FAS (CD95) expression on primary small intestinal IECs (EpCAM^{high} living cells) from mice with the indicated genotypes as assessed by FACS (n = 2-3 mice per genotype).

(H) Relative deletion of the loxP flanked sequence in the *Tnfrsf10b* (*Trailr2)* coding region in genomic DNA from small intestinal IECs of 2 to 3 mice with the indicated genotypes, as assessed by the relative amplification of the deleted locus area versus a control genomic region.

All scale bars represent 100µm.

Supplemental Data Figure 4

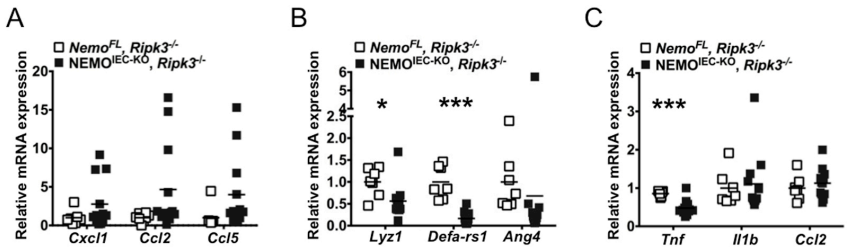

Figure S4 related to Figure 5

Deletion of RIPK3 ameliorates inflammation in colons of NEMO^{IEC-KO} mice but does not affect Paneth cell deficiency

(A) Graph depicting mRNA levels of the indicated genes in the colon of NEMO^{IEC-KO}, *Ripk3*$^{-/-}$ and *Nemo*^{FL}, *Ripk3*$^{-/-}$ mice (n = 8-12 mice per genotype).

(B, C) Graphs depicting mRNA levels of the indicated genes in the ileum of NEMO^{IEC-KO}, *Ripk3*$^{-/-}$ and *Nemo*^{FL}, *Ripk3*$^{-/-}$ mice (n = 7-12 mice per genotype).

Supplemental Data Figure 5

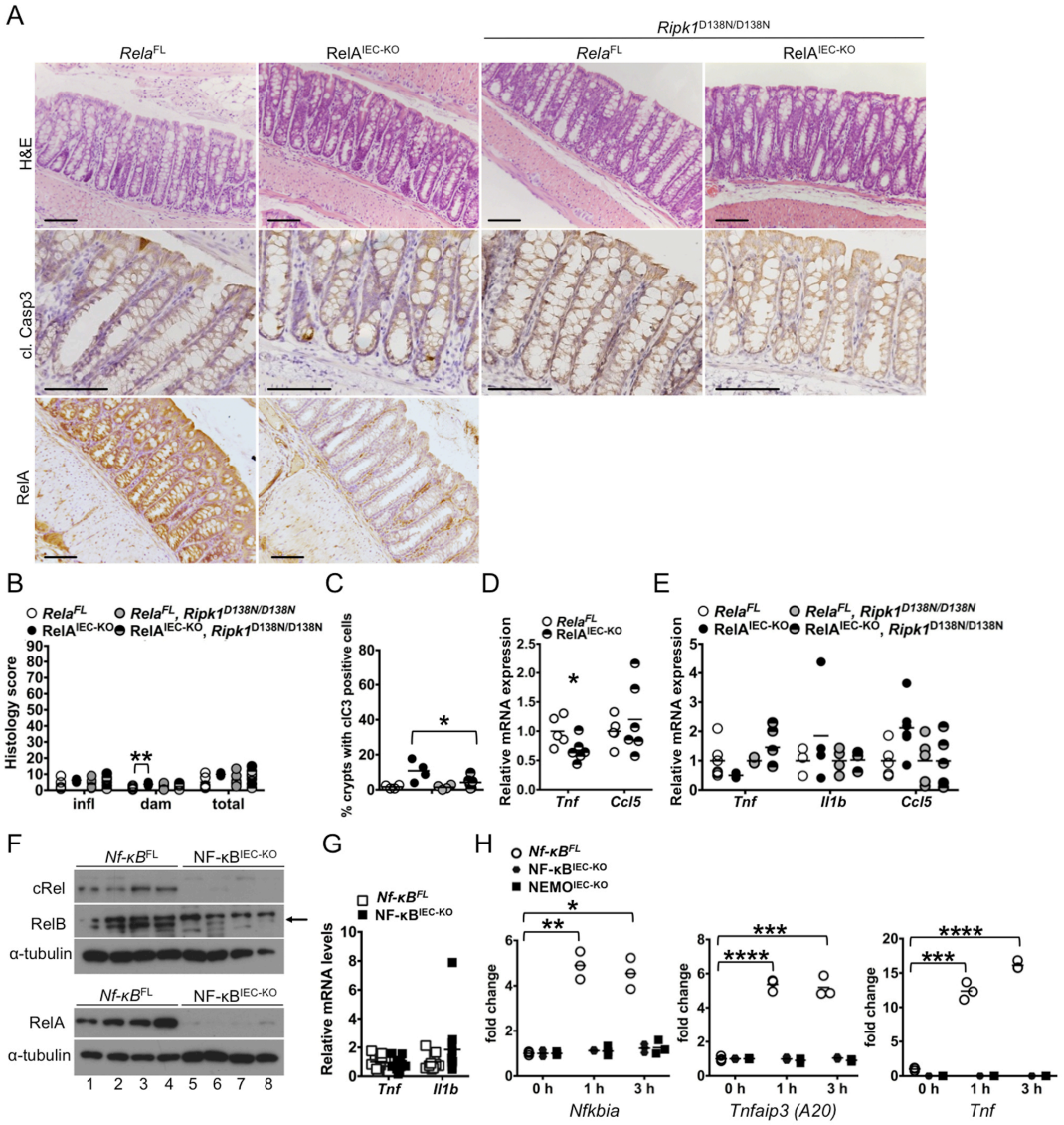

Figure S5 related to Figure 7

RelA$^{IEC\text{-}KO}$ mice do not develop spontaneous colitis

(A) Representative images of colon sections from RelA$^{IEC\text{-}KO}$ and *Rela*^{FL} littermates and RelA$^{IEC\text{-}KO}$, *Ripk1*$^{D138N/D138N}$ and *Rela*^{FL}, *Ripk1*$^{D138N/D138N}$ littermate mice stained with H&E or immunostained for cl. casp3 or RelA.

(B) Graph depicting histopathological scores of colon sections from RelA$^{IEC\text{-}KO}$ and *Rela*^{FL} littermates and RelA$^{IEC\text{-}KO}$, *Ripk1*$^{D138N/D138N}$ and *Rela*^{FL}, *Ripk1*$^{D138N/D138N}$ littermate mice (n = 5-6 mice per genotype).

(C) Graph depicting percentage of crypts with cl. casp. 3 stained cells on colon sections from RelA$^{IEC\text{-}KO}$ and *Rela*^{FL}, RelA$^{IEC\text{-}KO}$, *Ripk1*$^{D138N/D138N}$ and *Rela*^{FL}, *Ripk1*$^{D138N/D138N}$ mice (n = 4-6 mice per genotype).

(D) Graph depicting mRNA levels of the indicated genes in the colon of RelA$^{IEC\text{-}KO}$ and *Rela*^{FL} mice (n = 5-6 mice per genotype).

(E) Graph depicting mRNA levels of the indicated genes in ilea from RelA$^{IEC\text{-}KO}$, *Rela*^{FL}, RelA$^{IEC\text{-}KO}$, *Ripk1*$^{D138N/D138N}$ and *Rela*^{FL}, *Ripk1*$^{D138N/D138N}$ mice (n = 3-6 mice per genotype).

(F) Immunoblot analysis of protein extracts from primary small intestinal IECs from *Nf-κB*^{FL} and NF-κB$^{IEC\text{-}KO}$ mice with the indicated antibodies. Note that the extract in line 6 is derived from a heterozygous *relb*$^{FL/WT}$ mouse thus showing reduced levels of RelB protein. Arrow indicates specific band for RelB.

(G) Graph depicting mRNA levels of the indicated genes in the ileum of *Nf-κB*^{FL} and NF-κB$^{IEC\text{-}KO}$ littermates (n = 11-12 mice per genotype).

(H) Graphs depicting the fold change of mRNA levels of the indicated NF-κB target genes compared to unstimulated controls in small intestinal organoids from *Nf*-κ*B*^{FL}, NF-κB^{IEC-KO} and NEMO^{IEC-KO} mice after 1 h and 3 h stimulation with 5 ng/ml murine recombinant TNF. *Tnf* mRNA was not detectable at any time point in organoids from NF-κB^{IEC-KO} and NEMO^{IEC-KO} mice. Representative data from one of two independent experiments shown.

All scale bars represent 100μm.

Supplemental Data Figure 6

A

Parental genotypes	F: *Rela*$^{WT/-}$ X M: *Rela*$^{WT/-}$		
Born mice	expected	observed	
Genotype	%	n	%
Rela$^{WT/WT}$	25.0%	11	34.4%
Rela$^{WT/-}$	50.0%	21	65.6%
Rela$^{-/-}$	25.0%	0	0%
Total		32	
E12.5 – E14.5 Embryos	expected	observed	
Genotype	%	n	%
Rela$^{WT/WT}$	25.0%	9	28.1%
Rela$^{WT/-}$	50.0%	14	43.8%
Rela$^{-/-}$	25.0%	9	28.1%
Total		32	

B

Parental genotypes	F: *Rela*$^{WT/-}$, *Tnfr1*$^{-/-}$ X M: *Rela*$^{WT/-}$, *Tnfr1*$^{-/-}$			Day of death
Born mice	expected	observed		
Genotype	%	n	%	
Rela$^{WT/WT}$, *Tnfr1*$^{-/-}$	25.0%	4	14.3%	
Rela$^{WT/-}$, *Tnfr1*$^{-/-}$	50.0%	20	71,4%	
Rela$^{-/-}$, *Tnfr1*$^{-/-}$	25.0%	4	14.3%	P33, 3x sacrifice P2
Total		28		

C

Parental genotypes	F: *Rela*$^{WT/-}$, *Ripk1*$^{D138N/D138N}$ X M: *Rela*$^{WT/-}$, *Ripk1*$^{D138N/D138N}$			Day of death
Born mice	expected	observed		
Genotype	%	n	%	
Rela$^{WT/WT}$, *Ripk1*$^{D138N/D138N}$	25.0%	12	26.7%	
Rela$^{WT/-}$, *Ripk1*$^{D138N/D138N}$	50.0%	26	57.8%	
Rela$^{-/-}$, *Ripk1*$^{D138N/D138N}$	25.0%	7	15.6%	3x P6; P12; P27; P33; P34
Total		45		
E12.5 – E14.5 Embryos	expected	observed		
Genotype	%	n	%	
Rela$^{WT/WT}$, *Ripk1*$^{D138N/D138N}$	25.0%	12	25.5%	
Rela$^{WT/-}$, *Ripk1*$^{D138N/D138N}$	50.0%	25	53.2%	
Rela$^{-/-}$, *Ripk1*$^{D138N/D138N}$	25.0%	10	21.3%	
Total		47		

D

Parental genotypes	F: *Rela*$^{WT/-}$, *Ripk1*$^{D138N/WT}$ X M: *Rela*$^{WT/-}$, *Ripk1*$^{D138N/D138N}$			Day of death
Born mice	expected	observed		
Genotype	%	n	%	
Rela$^{WT/WT}$, *Ripk1*$^{D138N/WT}$	12.5%	8	17.0%	
Rela$^{WT/WT}$, *Ripk1*$^{D138N/D138N}$	12.5%	9	19.1%	
Rela$^{WT/-}$, *Ripk1*$^{D138N/WT}$	25.0%	13	27.7%	
Rela$^{WT/-}$, *Ripk1*$^{D138N/D138N}$	25.0%	11	23.4%	
Rela$^{-/-}$, *Ripk1*$^{D138N/WT}$	12.5%	1	2.1%	P12
Rela$^{-/-}$, *Ripk1*$^{D138N/D138N}$	12.5%	5	10.6%	P17; P15; 3x sacrifice P20
Total		43		

E

Parental genotypes	F: *Nemo*$^{WT/-}$, *Ripk1*$^{D138N/D138N}$ or F: *Nemo*$^{FL/-}$, *Ripk1*$^{D138N/D138N}$ X M: *Ripk1*$^{D138N/D138N}$		
Born male mice	expected	observed	
Genotype	%	n	%
Nemo$^{WT/Y}$, *Ripk1*$^{D138N/D138N}$ or *Nemo*$^{FL/Y}$, *Ripk1*$^{D138N/D138N}$	50.0%	8	66.7%
Nemo$^{-/Y}$, *Ripk1*$^{D138N/D138N}$	50.0%	4	33.3%
Total		12	

Figure S6 related to Figure 6 and Figure 7

RIPK1 kinase activity mediates embryonic lethality of *Rela*$^{-/-}$ and *Nemo*$^{-/-}$ mice.

(A) Table showing the expected Mendelian frequency and the observed frequency of born offspring and E12.5-E14.5 embryos with the indicated genotypes from matings with *Rela*$^{WT/-}$ female (F) and *Rela*$^{WT/-}$ male (M) mice.

(B) Table showing the expected Mendelian frequency and the observed frequency of born offspring with the indicated genotypes from matings with *Rela*$^{WT/-}$, *Tnfr1*$^{-/-}$ female (F) and *Rela*$^{WT/-}$, *Tnfr1*$^{-/-}$ male (M) mice. The last column indicates the day of death or day of sacrifice of *Rela*$^{-/-}$, *Tnfr1*$^{-/-}$ offspring.

(C) Table showing the expected Mendelian frequency and the observed frequency of born offspring and E12.5-E14.5 embryos with the indicated genotypes from matings with *Rela*$^{WT/-}$, *Ripk1*$^{D138N/D138N}$ female (F) and *Rela*$^{WT/-}$, *Ripk1*$^{D138N/D138N}$ male (M) mice. The last column indicates the day of death or day of sacrifice of *Rela*$^{-/-}$, *Ripk1*$^{D138N/D138N}$ mice.

(D) Table showing the expected Mendelian frequency and the observed frequency of born offspring with the indicated genotypes from matings with *Rela*$^{WT/-}$, *Ripk1*$^{WT/D138N}$ female (F) and *Rela*$^{WT/-}$, *Ripk1*$^{D138N/D138N}$ male (M) mice. The last column indicates the day of death or day of sacrifice of *Rela*$^{-/-}$, *Ripk1*$^{D138N/D138N}$ and *Rela*$^{-/-}$, *Ripk1*$^{WT/D138N}$ mice.

(E) Table showing the expected Mendelian frequency and the observed frequency of born male offspring with the indicated genotypes from *Nemo*$^{WT/-}$, *Ripk1*$^{D138N/D138N}$ or *Nemo*$^{FL/-}$, *Ripk1*$^{D138N/D138N}$ females (F) mated to *Ripk1*$^{D138N/138N}$ males (M). *Nemo*$^{-/Y}$; *Ripk1*$^{D138N/D138N}$ pups were dead by P3.

Supplemental Experimental Procedures

Mice

Nemo^{FL} (*Ikbkg*^{fl}) (Schmidt-Supprian et al., 2000), *Rela*^{FL} (Luedde et al., 2008), *Fadd*^{FL} (Welz et al., 2011) and *Ripk1*$^{D138N/D138N}$ mice (Polykratis et al., 2014) were generated by gene targeting in C57BL/6 ES cells. *Villin*-cre (Madison et al., 2002), *Villin*-creER^{T2} (el Marjou et al., 2004), *Tnfr1*^{FL} (*Tnfrsf1a*^{fl}) (Van Hauwermeiren et al., 2013), *Trailr2*^{FL} (*Tnfrsf10b*^{fl})(Grosse-Wilde et al., 2008), *Fas*^{FL} (Hao et al., 2004), *Relb*^{FL} (Powolny-Budnicka et al., 2011), *c-Rel*^{FL} (Heise et al., 2014) and *Ripk3*$^{-/-}$ mice (Newton et al., 2004) were backcrossed for at least 10 generations into the C57BL/6 genetic background. *Villin*-creER^{T2} recombinase activity was induced by 5 daily intraperitoneal administrations of 1 mg tamoxifen dissolved in corn oil/DMSO. Littermates not carrying the Cre transgenes were used as controls in all experiments. Mice were analyzed at the age of 2-4 months. Mice of the indicated genotype were assigned at random to groups. Mouse studies were performed in a blinded fashion.

Quantitative RT–PCR

Total RNA was extracted with Trizol Reagent (Life Technologies) and RNeasy Columns (Qiagen). cDNA was prepared with Superscript III cDNA-synthesis Kit (Life Technologies). qRT–PCR was performed with TaqMan probes (Life Technologies) with TATA-box-binding protein (*Tbp*) and *Gapdh* serving as reference genes. Data were analyzed according to the ΔΔCT method and are presented in dot plot graphs as fold change (relative mRNA expression) relative to Cre negative littermates. Primer sequences are available upon request.

FACS analysis of Fas expression on IECs

Small intestinal IECs were isolated as described. For viability assessment cells were stained with fixable viability dye eFluor 780 (eBioscience), epithelial cells were identified as Epcam1-high with anti-EpCAM1/CD326-FITC (eBiosience) and expression of Fas was determined with anti-Fas/CD95-PE (BD Pharmingen) antibodies. Data were acquired with LSRFortessa, BD and analysis was performed with BD FACSDiva Software v8.0, plots were prepared with FlowJo Version 7.6.5 software.

Assessment of deletion efficiency of *Trailr2*

Deletion efficiency of *Trailr2* was assessed on genomic DNA isolated from small intestinal IECs as described before (Ehlken et al., 2014). Results are depicted as 1 – [2^ - (Ct deleted amplicon – Ct control amplicon)].

Histopathological evaluation of H&E stained tissue sections

Histopathological evaluation of tissue sections was performed on 3µm H&E stained intestinal tissue sections in a blinded fashion as described previously (Adolph et al., 2013). Inflammation scores are composed of four parameters, tissue damage scores are represented by the sum of three parameters that were multiplied with a factor taking into account the fraction of tissue being affected. In brief, inflammation was assessed by the presence of infiltrating mononuclear cells, polymorphonuclear cells and lymphocytic cells (scores from 0 to 3, with 0 absent, 1 mild, 2 moderate, 3 severe), and the localization of inflammatory infiltrates (0 absent, 1 mucosal, 2 submucosal, 3 transmural extending into muscularis and serosa, and 4 diffuse). For the evaluation of tissue damage four scores were ascribed to crypt hyperplasia, epithelial injury and death of epithelial cells (0 absent, 1 mild, 2 moderate and 3 severe). The sum of these inflammation or tissue damage scores were then multiplied by a factor according to the fraction of the tissue being affected: 1, < 10%; 2, 10-25%; 3, 25-50%; and 4, >50%. The total histological score represents the sum of inflammation and damage marks.

Paneth cell scores describe morphology and abundance of Paneth cells assessed on H&E stained paraffin sections. According to the extent of morphological alterations 5 scores were used to characterize Paneth cells describing cell shape and size, and the appearance of eosinophilic secretory granules. 0 characterizes normal, differentiated Paneth cells with well-formed roundish secretory granules; a score of 1 describes mild defects in secretory granule formation and mild alterations in cell shape; 2 indicates mild alterations in cell size and shape and moderate changes in granule appearance affecting less than half of the Paneth cells within a crypt; score 3 represents Paneth cells with more overt defects in their morphology involving more than half of the Paneth cells in a crypt; score 4 characterized severe Paneth cell abnormalities clearly detectable at lower power magnifications.

Five scores were employed to characterize relative Paneth cell numbers. 0 corresponds to normal Paneth cells numbers. A score of 1 characterizes a mild reduction in Paneth cell numbers per crypt. Score 2 corresponds to up to 25% reduction of Paneth cells per crypt, already noticeable at lower power magnifications. Score 3 describes an about 50% reduction in Paneth cells with most crypts still harboring Paneth cells. 4 was assigned when remaining Paneth cells accounted for less than 30% of Paneth cells in a wild type status (score 0) and stretches of crypts devoid of Paneth cells were identified.

Supplemental References

Adolph, T.E., Tomczak, M.F., Niederreiter, L., Ko, H.J., Bock, J., Martinez-Naves, E., Glickman, J.N., Tschurtschenthaler, M., Hartwig, J., Hosomi, S.*, et al.* (2013). Paneth cells as a site of origin for intestinal inflammation. Nature *503*, 272-276.

Ehlken, H., Krishna-Subramanian, S., Ochoa-Callejero, L., Kondylis, V., Nadi, N.E., Straub, B.K., Schirmacher, P., Walczak, H., Kollias, G., and Pasparakis, M. (2014). Death receptor-independent FADD signalling triggers hepatitis and hepatocellular carcinoma in mice with liver parenchymal cell-specific NEMO knockout. Cell Death Differ *21*, 1721-1732.

el Marjou, F., Janssen, K.P., Chang, B.H., Li, M., Hindie, V., Chan, L., Louvard, D., Chambon, P., Metzger, D., and Robine, S. (2004). Tissue-specific and inducible Cre-mediated recombination in the gut epithelium. Genesis *39*, 186-193.

Grosse-Wilde, A., Voloshanenko, O., Bailey, S.L., Longton, G.M., Schaefer, U., Csernok, A.I., Schutz, G., Greiner, E.F., Kemp, C.J., and Walczak, H. (2008). TRAIL-R deficiency in mice enhances lymph node metastasis without affecting primary tumor development. J Clin Invest *118*, 100-110.

Hao, Z., Hampel, B., Yagita, H., and Rajewsky, K. (2004). T cell-specific ablation of Fas leads to Fas ligand-mediated lymphocyte depletion and inflammatory pulmonary fibrosis. J Exp Med *199*, 1355-1365.

Heise, N., De Silva, N.S., Silva, K., Carette, A., Simonetti, G., Pasparakis, M., and Klein, U. (2014). Germinal center B cell maintenance and differentiation are controlled by distinct NF-kappaB transcription factor subunits. J Exp Med *211*, 2103-2118.

Luedde, T., Heinrichsdorff, J., de Lorenzi, R., De Vos, R., Roskams, T., and Pasparakis, M. (2008). IKK1 and IKK2 cooperate to maintain bile duct integrity in the liver. Proc Natl Acad Sci U S A *105*, 9733-9738.

Madison, B.B., Dunbar, L., Qiao, X.T., Braunstein, K., Braunstein, E., and Gumucio, D.L. (2002). Cis elements of the villin gene control expression in restricted domains of the vertical (crypt) and horizontal (duodenum, cecum) axes of the intestine. J Biol Chem *277*, 33275-33283.

Newton, K., Sun, X., and Dixit, V.M. (2004). Kinase RIP3 is dispensable for normal NF-kappa Bs, signaling by the B-cell and T-cell receptors, tumor necrosis factor receptor 1, and Toll-like receptors 2 and 4. Mol Cell Biol *24*, 1464-1469.

Polykratis, A., Hermance, N., Zelic, M., Roderick, J., Kim, C., Van, T.M., Lee, T.H., Chan, F.K., Pasparakis, M., and Kelliher, M.A. (2014). Cutting edge: RIPK1 Kinase inactive mice are viable and protected from TNF-induced necroptosis in vivo. J Immunol *193*, 1539-1543.

Powolny-Budnicka, I., Riemann, M., Tanzer, S., Schmid, R.M., Hehlgans, T., and Weih, F. (2011). RelA and RelB transcription factors in distinct thymocyte populations control lymphotoxin-dependent interleukin-17 production in gammadelta T cells. Immunity *34*, 364-374.

Schmidt-Supprian, M., Bloch, W., Courtois, G., Addicks, K., Israel, A., Rajewsky, K., and Pasparakis, M. (2000). NEMO/IKK gamma-deficient mice model incontinentia pigmenti. Mol Cell *5*, 981-992.

Van Hauwermeiren, F., Armaka, M., Karagianni, N., Kranidioti, K., Vandenbroucke, R.E., Loges, S., Van Roy, M., Staelens, J., Puimege, L., Palagani, A.*, et al.* (2013). Safe TNF-based antitumor therapy following p55TNFR reduction in intestinal epithelium. J Clin Invest *123*, 2590-2603.

Welz, P.S., Wullaert, A., Vlantis, K., Kondylis, V., Fernandez-Majada, V., Ermolaeva, M., Kirsch, P., Sterner-Kock, A., van Loo, G., and Pasparakis, M. (2011). FADD prevents RIP3-mediated epithelial cell necrosis and chronic intestinal inflammation. Nature *477*, 330-334.